Z. Angew. Math. Phys. 64 (2013), 1363–1386

0044-2275/13/041363-24
published online November 7, 2012
DOI 10.1007/s00033-012-0273-1

Zeitschrift für angewandte Mathematik und Physik ZAMP

Strain gradient solutions of half-space and half-plane contact problems

X.-L. Gao and S.-S. Zhou

Abstract. General solutions for the problems of an elastic half-space and an elastic half-plane, respectively, subjected to a symmetrically distributed normal force of arbitrary profile are analytically derived using a simplified strain gradient elasticity theory (SSGET) that contains one material length scale parameter. Mindlin's potential function method and Fourier transforms are employed in the formulation, and the half-space and half-plane contact problems are solved in a unified manner. The specific solutions for the problems of a half-space/plane subjected to a concentrated normal force or a uniformly distributed normal force are obtained by directly applying the general solutions, which recover the existing classical elasticity-based solutions of the Flamant and Boussinesq problems as special cases. In addition, the indentation problems of an elastic half-space indented by a flat-ended cylindrical punch, a spherical punch, and a conical punch, respectively, are solved using the general solutions, leading to hardness formulas that are indentation size- and material microstructure-dependent. Numerical results reveal that the displacement and stress fields in a half-space/plane given by the current SSGET-based solutions are smoother than those predicted by the classical elasticity-based solutions and do not exhibit the discontinuity and/or singularity displayed by the latter. Also, the indentation hardness values based on the newly obtained half-space solution are found to increase with decreasing indentation radius and increasing material length scale parameter, thereby explaining the microstructure-dependent indentation size effect.

Mathematics Subject Classification. 74A10 · 74B05 · 74M15.

Keywords. Strain gradient elasticity · Contact mechanics · Flamant problem · Boussinesq problem · Size effect · Indentation hardness · Potential function · Punch.

1. Introduction

Due to a lack of any material length scale parameter, classical continuum theories cannot explain size effects exhibited by many materials at the micron and nanometer scales (e.g., [2,7,21,37,45]). Hence, higher-order elasticity theories have been developed to interpret microstructure-dependent size effects on elastic properties, which include the Cosserat theory [8], couple stress theories (e.g., [23,32,36,38,46,47,50]), and strain gradient elasticity theories (e.g., [12,15,33–35]).

The general strain gradient elasticity theory of Mindlin [33] for an isotropic material contains 16 material parameters in addition to the two Lamé constants, which are challenging to determine experimentally (e.g., [24]). Difficulties also arise from having to deal with the associated higher-order equilibrium equations and extra boundary conditions. Owing to these challenges, Mindlin's general theory has not been widely used in modeling size-dependent material responses.

Simplified versions of the strain gradient elasticity theory of Mindlin [33] have been suggested (e.g., [1,12,17,48]). Such simplified models are mathematically more tractable and are quite desirable in view of the formidable experimental efforts required in determining additional material parameters.

These simplified strain gradient elasticity theories have been employed to analyze various problems in solid mechanics, such as fracture [17,42], mechanics of defects [25,26], thick-walled shells [15,16], and Eshelby-type inclusion problems [10–14,29–31]. The two-dimensional (2-D) and three-dimensional (3-D) problems of a point force in an infinite elastic body have also been studied using simplified strain gradient elasticity theories (e.g., [11,14,22,25,39]).

However, the Flamant and Boussinesq problems have not been satisfactorily explored using such theories. The 2-D Flamant problem was analyzed in [27] and [52] employing the simplified strain gradient elasticity theories suggested in [1] and [48], respectively. But these solutions are not exact, since the boundary conditions (BCs) used are not complete or variationally consistent. The plane strain Flamant problem was recently re-examined in [18] using correct BCs and a dipolar gradient elasticity theory (a simplified version of the general theory of Mindlin [33]). Like in [27,52], Georgiadis and Anagnostou [18] also applied the Fourier transform method to directly solve the displacement-equations of equilibrium, which are fourth-order partial differential equations (PDEs). Due to the difficulties in evaluating some integrals involved, the solution for the 2-D Flamant problem provided in [18] is not in a closed form. For 3-D contact problems, no analytical solution that uses correct and complete boundary conditions based on a strain gradient elasticity theory has been reported.

In the current paper, the 3-D problem of a half-space subjected to an axisymmetrically distributed normal force of arbitrary profile is solved together with the corresponding 2-D half-plane problem in a unified manner using a simplified strain gradient elasticity theory (SSGET) that contains only one material length scale parameter. The potential function method of Mindlin [33] and Fourier transforms are utilized in deriving the general solutions. The specific solutions for the problems of a half-space/plane subjected to a concentrated normal force or a uniformly distributed normal force are then obtained by directly applying the general solutions. The solutions of the Flamant and Boussinesq problems based on classical elasticity are recovered as special cases of the SSGET-based solutions for the concentrated normal force problems. By using the general solutions, the indentation problems of an elastic half-space indented by a flat-ended cylindrical punch, a spherical punch, and a conical punch, respectively, are solved, leading to size- and microstructure-dependent hardness formulas. To quantitatively illustrate the newly obtained solutions and formulas, numerical results are also presented.

2. Potential function method

2.1. Simplified strain gradient elasticity theory

In a first-order strain gradient elasticity theory, the strain energy density function w has the form:

$$w = w(\varepsilon_{ij}, \kappa_{ijk}), \tag{1}$$

where ε_{ij} and κ_{ijk} are, respectively, the components of the infinitesimal strain and strain gradient tensors defined by

$$\varepsilon_{ij} = \frac{1}{2}\left(u_{i,j} + u_{j,i}\right), \quad \kappa_{ijk} = \varepsilon_{ij,k}, \tag{2a,b}$$

with u_i being the components of the displacement vector.

For an isotropic linear elastic material, the general expression of w can be written as [12,35]

$$w = \frac{1}{2}\lambda\varepsilon_{ii}\varepsilon_{jj} + \mu\varepsilon_{ij}\varepsilon_{ij} + c_1\kappa_{ijj}\kappa_{ikk} + c_2\kappa_{iik}\kappa_{kjj} + c_3\kappa_{iik}\kappa_{jjk} + c_4\kappa_{ijk}\kappa_{ijk} + c_5\kappa_{ijk}\kappa_{kji}, \tag{3}$$

where λ and μ are Lamé's constants in classical elasticity, and $c_1 - c_5$ are additional material constants. In Eqs. (1)–(3) and throughout the paper, the summation convention and standard index notation are used, with the Greek indices running from 1 to 2 and the Latin indices from 1 to 3 unless otherwise indicated.

As stated in [12], when $c_1 = c_2 = c_5 = 0, c_3 = \frac{1}{2}\lambda l^2$ and $c_4 = \mu l^2$, Eq. (3) reduces to

$$w = \frac{1}{2}\lambda\varepsilon_{ii}\varepsilon_{jj} + \mu\varepsilon_{ij}\varepsilon_{ij} + l^2\left(\frac{1}{2}\lambda\kappa_{iik}\kappa_{jjk} + \mu\kappa_{ijk}\kappa_{ijk}\right), \tag{4}$$

which is the strain energy density function adopted in the simplified strain gradient elasticity theory (SSGET) (e.g., [1,15,26]). In Eq. (4), l is a material length scale parameter having the dimension of length, which can be determined experimentally or computationally (e.g., [12,24,43]).

It follows from Eq. (4) that the Cauchy stress, τ_{ij}, and the double stress, μ_{ijk}, are given by

$$\tau_{ij} = \frac{\partial w}{\partial \varepsilon_{ij}} = \lambda \varepsilon_{ll}\delta_{ij} + 2\mu\varepsilon_{ij} = \tau_{ji},$$
$$\mu_{ijk} = \frac{\partial w}{\partial \kappa_{ijk}} = l^2\left(\lambda\kappa_{llk}\delta_{ij} + 2\mu\kappa_{ijk}\right) = l^2\tau_{ij,k}. \tag{5a,b}$$

The total stress, σ_{ij}, is related to the Cauchy stress through [15]

$$\sigma_{ij} = \tau_{ij} - \mu_{ijk,k} = (1 - l^2\nabla^2)\tau_{ij}, \tag{6}$$

and the equilibrium equations have the form:

$$\sigma_{ij,j} + f_i = 0, \tag{7}$$

where f_i are the components of the body force.

Equation (7) can be rewritten in terms of the displacement vector $\mathbf{u} = u_i\mathbf{e}_i$ as [15]

$$(1 - l^2\nabla^2)\left[(\lambda + 2\mu)\nabla(\nabla\cdot\mathbf{u}) - \mu\nabla\times(\nabla\times\mathbf{u})\right] + \mathbf{f} = \mathbf{0}, \tag{8}$$

which is the displacement-equation of equilibrium based on the SSGET. In Eq. (8), $\nabla, \nabla\cdot, \nabla\times$, and ∇^2 denote, respectively, the gradient, divergence, curl, and Laplacian of the indicated quantity.

2.2. Potential function method of Mindlin

The displacement-equation of equilibrium in the general strain gradient elasticity theory of Mindlin [33] has the form:

$$(\lambda + 2\mu)(1 - l_1^2\nabla^2)\nabla(\nabla\cdot\mathbf{u}) - \mu(1 - l_2^2\nabla^2)\nabla\times(\nabla\times\mathbf{u}) + \mathbf{f} = \mathbf{0}, \tag{9}$$

where l_1 and l_2 are two material length scale parameters that can be related to the material constants c_i by (e.g., [22,43])

$$l_1^2 = \frac{2(c_1 + c_2 + c_3 + c_4 + c_5)}{\lambda + 2\mu}, \quad l_2^2 = \frac{(c_3 + 2c_4 + c_5)}{2\mu}. \tag{10}$$

Clearly, Eq. (9) reduces to Eq. (8) when $l_1 = l_2 = l$.

The general solution of Eq. (9) is given by [33]

$$\mathbf{u} = \mathbf{B} - l_2^2\nabla(\nabla\cdot\mathbf{B}) - \frac{1}{2}(\alpha - l_1^2\nabla^2)\nabla\left[\mathbf{r}\cdot(1 - l_2^2\nabla^2)\mathbf{B} + B_0\right], \tag{11a}$$

where $\alpha = 1/[2(1-\nu)]$, $\mathbf{r}$ is the position vector, and $\mathbf{B}$ and B_0 are, respectively, a vector potential function and a scalar potential function satisfying

$$\mu(1 - l_2^2\nabla^2)\nabla^2\mathbf{B} = -\mathbf{f},$$
$$\mu(1 - l_1^2\nabla^2)\nabla^2 B_0 = \mathbf{r}\cdot(1 - l_1^2\nabla^2)\mathbf{f} - 4l_1^2\nabla\cdot\mathbf{f}. \tag{11b,c}$$

In the absence of body forces, $\mathbf{f} = \mathbf{0}$ and Eqs. (11b,c) become

$$\mu(1 - l_2^2\nabla^2)\nabla^2\mathbf{B} = \mathbf{0},$$
$$\mu(1 - l_1^2\nabla^2)\nabla^2 B_0 = 0. \tag{11d,e}$$

When $l_1 = l_2 = 0$, Eq. (9) reduces to the Navier displacement-equation of equilibrium in classical elasticity, Eq. (11a) recovers the general solution of the Navier equation, and $\mathbf{B}$ and B_0 defined in Eqs. (11b,c) become the well-known Papkovitch-Neuber potential functions (e.g., [53]).

When $l_1 = 0$ and $l_2 = l$, Eq. (9) reads, with $\mathbf{f} = \mathbf{0}$,

$$\mu\nabla^2\mathbf{u} + (\lambda + \mu)\nabla(\nabla\cdot\mathbf{u}) + \mu l^2\nabla^2[\nabla\times(\nabla\times\mathbf{u})] = \mathbf{0}, \tag{12}$$

and Eqs. (11a,d,e) reduce to

$$\mathbf{u} = \mathbf{B} - l^2\nabla(\nabla\cdot\mathbf{B}) - \frac{\alpha}{2}\nabla\left[\mathbf{r}\cdot(1-l^2\nabla^2)\mathbf{B} + B_0\right], \tag{13a}$$

$$\begin{aligned}\mu(1-l^2\nabla^2)\nabla^2\mathbf{B} &= \mathbf{0},\\ \mu\nabla^2 B_0 &= 0.\end{aligned} \tag{13b,c}$$

Note that in reaching Eq. (12) use has been made of the identity: $\nabla(\nabla\cdot\mathbf{u}) - \nabla\times(\nabla\times\mathbf{u}) = \nabla^2\mathbf{u}$ (e.g., [38]). Equations (12) and (13a,b,c) are the same as those originally provided in [36] in the absence of body forces and body couples. The solution given in Eqs. (12) and (13a,b,c) was adopted in [9] to solve axisymmetric contact problems.

Since Eq. (9) becomes identical to Eq. (8) when $l_1 = l_2 = l$, the general solution of Eq. (8) can be readily obtained from Eqs. (11a,b,c) with $l_1 = l_2 = l$ as

$$\mathbf{u} = \mathbf{B} - l^2\nabla(\nabla\cdot\mathbf{B}) - \frac{1}{2}(\alpha - l^2\nabla^2)\nabla\left[\mathbf{r}\cdot(1-l^2\nabla^2)\mathbf{B} + B_0\right], \tag{14a}$$

with

$$\begin{aligned}(1-l^2\nabla^2)\nabla^2\mathbf{B} &= \mathbf{0},\\ (1-l^2\nabla^2)\nabla^2 B_0 &= 0\end{aligned} \tag{14b,c}$$

in the absence of body forces.

The use of Mindlin's potential function method has reduced the problem of solving the fourth-order partial differential equations in Eq. (8) (with $\mathbf{f} = \mathbf{0}$) to the problem of finding the potential functions $\mathbf{B}$ and B_0 satisfying Eqs. (14b,c). This approach is adopted in the current study to solve half-space (3-D) and half-plane (2-D) contact problems, which is more advantageous than that employed in [18,27,52] in solving the 2-D Flamant problem, where the Fourier transform method was directly applied to solve the fourth-order displacement-equations of equilibrium.

3. Formulation

The half-plane and half-space contact problems considered in this study are shown in Fig. 1. It is assumed that body forces are absent so that Eqs. (14a,b,c) give the solution of Eq. (8), which is the final governing equation in the SSGET.

For a half-space (occupying $x_3 \geq 0$) subjected to an axisymmetrically distributed normal force, the vector potential function $\mathbf{B}$ takes the form $(0, 0, B_3)$ and the scalar potential function B_0 is non-zero (e.g., [9,53]). As a result, the displacement components in this case can be obtained from Eq. (14a) as

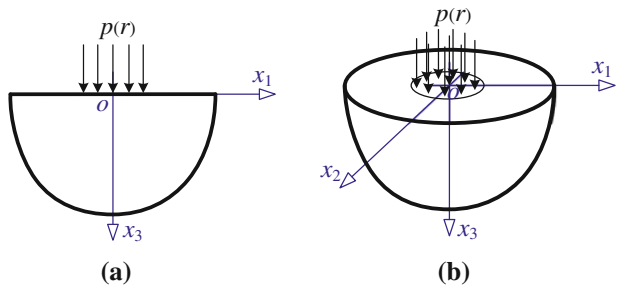

FIG. 1. A half-plane (**a**) and a half-space (**b**) subjected to a symmetrically distributed normal force of arbitrary profile

$$u_\beta = -l^2 B_{3,3\beta} - \frac{1}{2}(\alpha - l^2\nabla^2)\left[x_3(1-l^2\nabla^2)B_3 + B_0\right]_{,\beta},$$
$$u_3 = B_3 - l^2 B_{3,33} - \frac{1}{2}(\alpha - l^2\nabla^2)\left[x_3(1-l^2\nabla^2)B_3 + B_0\right]_{,3}, \tag{15a,b}$$

where B_3 and B_0 satisfy

$$\begin{aligned}(1-l^2\nabla^2)\nabla^2 B_3 = 0,\\ (1-l^2\nabla^2)\nabla^2 B_0 = 0,\end{aligned} \tag{15c,d}$$

which are directly obtained from Eqs. (14b,c).

3.1. Boundary conditions

The general form of boundary conditions (BCs) in the SSGET was obtained in [15] using a variational formulation based on the principle of minimum total potential energy, which reads

$$\left.\begin{aligned}\sigma_{ij}n_j - (\mu_{ijk}n_k)_{,j} + (\mu_{ijk}n_k n_l)_{,l}n_j = \bar{t}_i \ \text{ or } u_i = \overline{u_i}\\ \mu_{ijk}n_j n_k = \overline{q_i} \ \text{ or } u_{i,l}n_l = \overline{\frac{\partial u_i}{\partial n}}\end{aligned}\right\} \quad \text{on} \quad \partial\Omega, \tag{16}$$

where t_i and q_i are, respectively, the components of the Cauchy traction vector and double stress traction vector (see [12] for the general expressions of t_i and q_i), $\partial\Omega$ is the smooth boundary surface of the domain Ω occupied by the elastic body satisfying Eq. (8), n_i are the components of the unit outward normal vector on $\partial\Omega$, and the overhead bar represents the prescribed value.

For the current half-space problem, $\bar{\mathbf{t}} = p\mathbf{e}_3$ and $\overline{\mathbf{q}} = \mathbf{0}$ on $x_3 = 0$. Then, it follows from Eqs. (5a,b), (6) and (16) that, with $\mathbf{n} = -\mathbf{e}_3$,

$$\left.\begin{aligned}p + (1-l^2\nabla^2)\tau_{33} = 0,\\ (1-l^2\nabla^2)\tau_{\alpha 3} - l^2(\tau_{\alpha 1,31} + \tau_{\alpha 2,32}) = 0,\\ l^2\tau_{i3,3} = 0\end{aligned}\right\} \quad \text{on } x_3 = 0, \tag{17a-c}$$

where $p = p(r)$ and use has been made of Eq. (17c) in reaching Eq. (17a).

For the half-plane (plane strain) problem (see Fig. 1a), Eqs. (17a-c) become, with $\tau_{21} = \tau_{23} = 0$ and $\tau_{22} = \tau_{22}(x_1, x_3)$,

$$\left.\begin{aligned}p + (1-l^2\nabla^2)\tau_{33} = 0,\\ (1-l^2\nabla^2)\tau_{31} - l^2\tau_{11,31} = 0,\\ l^2\tau_{13,3} = 0,\\ l^2\tau_{33,3} = 0\end{aligned}\right\} \quad \text{on } x_3 = 0, \tag{18a-d}$$

which can be readily shown to be the same as the BCs used in [18] for the plane strain half-plane problem when p is a concentrated normal force acting at $(x_1, x_3) = (0, 0)$. Clearly, when $l = 0$, Eqs. (17a-c) reduce to $\tau_{i3} = -p\delta_{i3}$ on $x_3 = 0$, which are the BCs for the half-space problem based on classical elasticity (e.g., [54]).

The BCs in Eqs. (17a-c) or Eqs. (18a-d) will be used to determine the constants involved in the potential functions B_3 and B_0, which are to be obtained from solving Eqs. (15c,d).

3.2. Solutions in the Fourier domain

The Fourier transform and Hankel transform methods have been widely used to solve half-space/plane contact mechanics problems based on classical elasticity and surface elasticity (e.g., [4,19,41,51,53]). The Fourier transform method is employed herein to solve the half-space and half-plane contact problems that have been formulated in Sect. 3.1 using the SSGET and Mindlin's potential function method.

The Fourier transform pair is given by

$$\overline{f}(\xi) = \int_{-\infty}^{\infty} f(x) e^{-i\xi x} \mathrm{d}x,$$
$$f(x) = \frac{1}{2\pi} \int_{-\infty}^{\infty} \overline{f}(\xi) e^{i\xi x} \mathrm{d}\xi, \tag{19a,b}$$

and the double Fourier transform pair is defined as

$$\overline{f}(\xi_1, \xi_2) = \int_{-\infty}^{\infty} \int_{-\infty}^{\infty} f(x_1, x_2) e^{-i\xi_\alpha x_\alpha} \mathrm{d}x_1 \mathrm{d}x_2,$$
$$f(x_1, x_2) = \frac{1}{(2\pi)^2} \int_{-\infty}^{\infty} \int_{-\infty}^{\infty} \overline{f}(\xi_1, \xi_2) e^{i\xi_\alpha x_\alpha} \mathrm{d}\xi_1 \mathrm{d}\xi_2, \tag{20a,b}$$

where the overhead bar denotes the function in the transformed space and i is the imaginary unit satisfying $i^2 = -1$.

Taking Fourier transforms (see Eq. (20a)) on Eq. (15c) and Eq. (15d), respectively, yields

$$l^2 \frac{\partial^4 \overline{B}_3}{\partial x_3^4} - (1 + 2l^2\xi^2) \frac{\partial^2 \overline{B}_3}{\partial x_3^2} + (1 + l^2\xi^2)\xi^2 \overline{B}_3 = 0,$$
$$l^2 \frac{\partial^4 \overline{B}_0}{\partial x_3^4} - (1 + 2l^2\xi^2) \frac{\partial^2 \overline{B}_0}{\partial x_3^2} + (1 + l^2\xi^2)\xi^2 \overline{B}_0 = 0, \tag{21a,b}$$

where $\xi^2 = \xi_\alpha \xi_\alpha$. The solutions of Eqs. (21a,b) give, for the displacement $\mathbf{u}$ (and thus B_3 and B_0) to be finite at $x_3 \to \infty$,

$$\overline{B}_0 = A e^{-x_3|\xi|} + B e^{-x_3\zeta},$$
$$\overline{B}_3 = C e^{-x_3|\xi|} + D e^{-x_3\zeta}, \tag{22a,b}$$

where $\zeta \equiv \sqrt{\xi^2 + \frac{1}{l^2}}$, and A, B, C and D are unknowns to be determined from the BCs.

Next, performing Fourier transforms (see Eq. (20a)) on Eqs. (15a,b) and then using Eqs. (22a,b) result in the displacement components in the Fourier domain for the half-space problem as

$$\overline{u}_\beta = -\frac{i}{2}\xi_\beta \left\{ \alpha \left(C x_3 + A \right) e^{-x_3|\xi|} - \left[(1-\alpha) B + 2Dl^2\zeta \right] e^{-x_3\zeta} \right\},$$
$$\overline{u}_3 = \frac{1}{2} \left[(2-\alpha)C + \alpha |\xi| \left(C x_3 + A \right) \right] e^{-x_3|\xi|} - \frac{1}{2} \left[(1-\alpha) B\zeta + 2Dl^2\xi^2 \right] e^{-x_3\zeta}. \tag{23a,b}$$

These expressions also hold for the plane strain half-plane problem except that ξ_1 in Eqs. (23a,b) needs to be replaced by ξ. That is, the displacement components for the half-plane problem in the transformed space are given by

$$\overline{u}_1 = -\frac{i}{2}\xi \left\{ \alpha \left(C x_3 + A \right) e^{-x_3|\xi|} - \left[(1-\alpha) B + 2Dl^2\zeta \right] e^{-x_3\zeta} \right\},$$
$$\overline{u}_2 = 0,$$
$$\overline{u}_3 = \frac{1}{2} \left[(2-\alpha)C + \alpha |\xi| \left(C x_3 + A \right) \right] e^{-x_3|\xi|} - \frac{1}{2} \left[(1-\alpha) B\zeta + 2Dl^2\xi^2 \right] e^{-x_3\zeta}. \tag{24a-c}$$

It then follows from Eqs. (23a,b), (2a), (5a) and (20a) that the Cauchy stress components in the Fourier domain for the half-space problem are

$$
\begin{aligned}
\frac{\overline{\tau}_{\beta\beta}}{\mu} &= \alpha\left[-2\nu C\left|\xi\right| + (Cx_3 + A)\xi_\beta^2\right] e^{-x_3|\xi|} + \left\{B\left[\alpha\nu l^{-2} - (1-\alpha)\xi_\beta^2\right] - 2Dl^2\xi_\beta^2\zeta\right\} e^{-x_3\zeta},\\
\frac{\overline{\tau}_{12}}{\mu} &= \xi_1\xi_2\left\{\alpha(Cx_3 + A)e^{-x_3|\xi|} - \left[(1-\alpha)B + 2Dl^2\zeta\right] e^{-x_3\zeta}\right\},\\
\frac{\overline{\tau}_{\beta 3}}{\mu} &= i\xi_\beta\left\{\left[(1-\alpha)C + \alpha(Cx_3 + A)\left|\xi\right|\right] e^{-x_3|\xi|} - \left[(1-\alpha)B\zeta + D\left(1 + 2l^2\xi^2\right)\right] e^{-x_3\zeta}\right\},\\
\frac{\overline{\tau}_{33}}{\mu} &= -\left[C\left|\xi\right| + \alpha(Cx_3 + A)\xi^2\right] e^{-x_3|\xi|} + \left\{B\left[\frac{1}{2}l^{-2} + (1-\alpha)\xi^2\right] + 2Dl^2\xi^2\zeta\right\} e^{-x_3\zeta}.
\end{aligned}
\tag{25a-d}
$$

Note that no summation is implied on β in Eq. (25a).

For the plane strain half-plane problem, the non-zero stress components in the Fourier domain can be obtained from Eqs. (25a-d) as, after replacing ξ_1 by ξ and setting $\xi_2 = 0$,

$$
\begin{aligned}
\frac{\overline{\tau}_{11}}{\mu} &= \alpha\left[-2\nu C\left|\xi\right| + (Cx_3 + A)\xi^2\right] e^{-x_3|\xi|} + \left\{B\left[\alpha\nu l^{-2} - (1-\alpha)\xi^2\right] - 2Dl^2\xi^2\zeta\right\} e^{-x_3\zeta},\\
\frac{\overline{\tau}_{13}}{\mu} &= i\xi\left\{\left[(1-\alpha)C + \alpha(Cx_3 + A)\left|\xi\right|\right] e^{-x_3|\xi|} - \left[(1-\alpha)B\zeta + D\left(1 + 2l^2\xi^2\right)\right] e^{-x_3\zeta}\right\},\\
\frac{\overline{\tau}_{33}}{\mu} &= -\left[C\left|\xi\right| + \alpha(Cx_3 + A)\xi^2\right] e^{-x_3|\xi|} + \left\{B\left[\frac{1}{2}l^{-2} + (1-\alpha)\xi^2\right] + 2Dl^2\xi^2\zeta\right\} e^{-x_3\zeta},\\
\frac{\overline{\tau}_{22}}{\mu} &= \nu\alpha\left(-2C\left|\xi\right| e^{-x_3|\xi|} + Bl^{-2}e^{-x_3\zeta}\right).
\end{aligned}
\tag{26a-d}
$$

It can be readily verified that with $\alpha = 1/[2(1-\nu)]$, the normal stress components listed in Eqs. (26a,c,d) satisfy the relation $\overline{\tau}_{22} = \nu(\overline{\tau}_{11} + \overline{\tau}_{33})$, as expected for a plane strain problem.

Taking Fourier transforms (see Eq. (20a) and Eq. (19a)) on Eqs. (17a-c) and Eqs. (18a-d), respectively, and then using Eqs. (25a-d) and Eqs. (26a-c) in the resulting equations will lead to the BCs in the Fourier domain for the half-space and half-plane problems, respectively. These BCs, which happen to have the same form for the two problems, are given by

$$
\begin{aligned}
&\alpha\mu\xi^2 A + \mu\left|\xi\right|(1 + 2\alpha l^2\xi^2)C = \overline{p},\\
&\alpha l^2\left|\xi\right|\zeta^2 A + \left[\alpha\nu + (\alpha-1)l^2\xi^2\right]\zeta B + (1-\alpha)l^2\zeta^2 C - 2l^4\xi^2\zeta^2 D = 0,\\
&\alpha l^2\left|\xi\right|^3 A - \left[\frac{1}{2} + (1-\alpha)l^2\xi^2\right]\zeta B + (1-\alpha)l^2\xi^2 C - 2l^4\xi^2\zeta^2 D = 0,\\
&-\alpha\xi^2 A + (1-\alpha)\zeta^2 B + (2\alpha - 1)\left|\xi\right| C + (1 + 2l^2\xi^2)\zeta D = 0,
\end{aligned}
\tag{27}
$$

where $\overline{p}$ is the image of the distributed normal force p in the Fourier domain. The solution of this linear algebraic equation system gives

$$
\begin{aligned}
A &= -\frac{2(1-\nu)\overline{p}}{\mu\xi^2\varphi(\xi)}\left[(1-2\nu)(1-\nu+2l^4\xi^2\zeta^2) + 4\nu l^4\zeta\left|\xi\right|^3\right], \quad B = \frac{4(1-\nu)l^4\xi^2\overline{p}}{\mu\varphi(\xi)},\\
C &= \frac{2(1-\nu)\overline{p}}{\mu\left|\xi\right|\varphi(\xi)}\left[1-\nu+2l^4\xi^2\zeta\left(\zeta-\left|\xi\right|\right)\right], \quad D = -\frac{(1-\nu)\overline{p}}{\mu\zeta\varphi(\xi)}\left(1 + 2l^2\xi^2\right),
\end{aligned}
\tag{28a-d}
$$

where

$$
\varphi(\xi) = (1-\nu)(1 + 2l^2\xi^2) + 2l^6\zeta^2\xi^2(\zeta - \left|\xi\right|)^2. \tag{28e}
$$

Note that A, B, C and D are all even functions of ξ and that $\varphi(\xi) \geq 1 - \nu$ regardless of the value of ξ.

Using Eqs. (28a-d) in Eqs. (23a,b) and (25a-d) will give the final expressions of the displacement and stress components in the Fourier domain for the half-space problem, and substituting Eqs. (28a-d) into Eqs. (24a-c) and (26a-d) will yield the displacement and stress expressions in the Fourier domain for the plane strain half-plane problem.

4. General solutions

To obtain the displacement and stress components in the physical space from the corresponding expressions in the Fourier domain derived in Section 3.2, inverse Fourier transforms can be applied, as shown below in this section.

4.1. Half-plane problem

For the half-plane problem with a symmetrically distributed normal force $p(r)$ (see Fig. 1a), $\overline{p}$ is an even function of ξ. It then follows from Eqs. (24a-c), (26a-d) and (28a-d) that $\overline{u}_1$ and $\overline{\tau}_{13}$ are odd functions of ξ, and $\overline{u}_3, \overline{\tau}_{11}, \overline{\tau}_{22}$ and $\overline{\tau}_{33}$ are even functions of ξ. Performing inverse Fourier transforms (see Eq. (19b)) on Eqs. (24a-c) and Eqs. (26a-d), respectively, gives, after using Eqs. (28a-d),

$$\begin{aligned} u_1 &= -\frac{1}{2\pi\mu}\int_0^\infty \frac{\overline{p}}{\xi\varphi(\xi)}\left(h_{11}e^{-x_3\xi}+h_{12}e^{-x_3\zeta}\right)\sin(\xi x_1)\mathrm{d}\xi,\\ u_2 &= 0,\\ u_3 &= \frac{1}{2\pi\mu}\int_0^\infty \frac{\overline{p}}{\xi\varphi(\xi)}\left(h_{21}e^{-x_3\xi}+h_{22}e^{-x_3\zeta}\right)\cos(\xi x_1)\mathrm{d}\xi, \end{aligned} \tag{29a-c}$$

and

$$\begin{aligned} \tau_{11} &= -\int_0^\infty \frac{\overline{p}}{\pi\varphi(\xi)}\left(g_{11}e^{-x_3\xi}+g_{12}e^{-x_3\zeta}\right)\cos(\xi x_1)\mathrm{d}\xi,\\ \tau_{13} &= \int_0^\infty \frac{\overline{p}}{\pi\varphi(\xi)}\left(g_{21}e^{-x_3\xi}+g_{22}e^{-x_3\zeta}\right)\sin(\xi x_1)\mathrm{d}\xi,\\ \tau_{33} &= -\int_0^\infty \frac{\overline{p}}{\pi\varphi(\xi)}\left(g_{31}e^{-x_3\xi}+g_{32}e^{-x_3\zeta}\right)\cos(\xi x_1)\mathrm{d}\xi,\\ \tau_{22} &= -\int_0^\infty \frac{\nu\overline{p}}{\pi\varphi(\xi)}\left[(g_{11}+g_{31})e^{-x_3\xi}+(g_{12}+g_{32})e^{-x_3\zeta}\right]\cos(\xi x_1)\mathrm{d}\xi, \end{aligned} \tag{30a-d}$$

where

$$\begin{aligned} h_{11} &= 1-\nu+2l^4\xi^2\zeta^2+(2\nu+x_3\xi)\left[\nu-1+2l^4\xi^2\zeta(\xi-\zeta)\right],\\ h_{12} &= -2l^2\xi^2\left(1-\nu+l^2\xi^2\right),\\ h_{21} &= 2(1-\nu)\left(1-\nu+\frac{1}{2}x_3\xi+2l^4\xi^2\zeta^2\right)+2l^4\xi^3\zeta\left[2\nu-3+x_3(\zeta-\xi)\right],\\ h_{22} &= 2l^2\xi^3\zeta^{-1}\left(l^2\xi^2+\nu\right), \end{aligned} \tag{31a-d}$$

and

$$\begin{aligned}
g_{11} &= (1-\nu+2l^4\xi^2\zeta^2)(1-x_3\xi)+2x_3l^4\xi^4\zeta,\\
g_{12} &= -2l^4\xi^2\zeta^2,\\
g_{21} &= x_3\xi(\nu-1)+2l^4\xi^3\zeta(1+x_3\xi-x_3\zeta),\\
g_{22} &= -\xi\zeta^{-1}(1-\nu+2l^4\xi^2\zeta^2),\\
g_{31} &= (1-\nu+2l^4\xi^2\zeta^2)(1+x_3\xi)-2(2+x_3\xi)l^4\xi^3\zeta,\\
g_{32} &= 2l^4\xi^4.
\end{aligned} \tag{32a-f}$$

On the loading surface $x_3 = 0$, Eqs. (29a,c) and (31a-d) give

$$u_1|_{x_3=0} = -\frac{1}{2\pi\mu}\int_0^\infty \frac{\overline{p}}{\xi\varphi(\xi)}\left[(1-\nu)(1-2\nu)-2\nu l^4\xi^2(\zeta-\xi)^2\right]\sin(\xi x_1)\mathrm{d}\xi, \tag{33a,b}$$

$$u_3|_{x_3=0} = \frac{1-\nu}{\pi\mu}\int_0^\infty \frac{\overline{p}}{\xi\varphi(\xi)}\left[1-\nu-l^2\xi^3\zeta^{-1}+2l^4\xi^2\zeta(\zeta-\xi)\right]\cos(\xi x_1)\mathrm{d}\xi,$$

and Eqs. (30a-d) yield

$$\begin{aligned}
\tau_{11}|_{x_3=0} &= -\frac{1-\nu}{\pi}\int_0^\infty \frac{\overline{p}}{\varphi(\xi)}\cos(\xi x_1)\mathrm{d}\xi,\\
\tau_{13}|_{x_3=0} &= -\frac{1-\nu}{\pi}\int_0^\infty \frac{\xi\overline{p}}{\zeta\varphi(\xi)}\sin(\xi x_1)\mathrm{d}\xi,\\
\tau_{33}|_{x_3=0} &= -\frac{1}{\pi}\int_0^\infty \frac{\overline{p}}{\varphi(\xi)}\left[1-\nu+2l^4\xi^2(\zeta-\xi)^2\right]\cos(\xi x_1)\mathrm{d}\xi,\\
\tau_{22}|_{x_3=0} &= -\frac{2\nu}{\pi}\int_0^\infty \frac{\overline{p}}{\varphi(\xi)}\left[1-\nu+2l^4\xi^3\left(\xi-\zeta\right)+l^2\xi^2\right]\cos(\xi x_1)\mathrm{d}\xi.
\end{aligned} \tag{34a-d}$$

4.2. Half-space problem

For the half-space problem with an axisymmetrically distributed normal force $p(r)$ (see Fig. 1b), applying inverse Fourier transforms (see Eq. (20b)) to Eqs. (23a,b) and (25a-d) and using Eqs. (28a-d) will lead to

$$\begin{aligned}
u_\beta &= -\frac{x_\beta}{4\pi\mu r}\int_0^\infty \frac{\overline{p}}{\varphi(\xi)}\left(h_{11}e^{-x_3\xi}+h_{12}e^{-x_3\zeta}\right)J_1(\xi r)\mathrm{d}\xi,\\
u_3 &= \frac{1}{4\pi\mu}\int_0^\infty \frac{\overline{p}}{\varphi(\xi)}\left(h_{21}e^{-x_3\xi}+h_{22}e^{-x_3\zeta}\right)J_0(\xi r)\mathrm{d}\xi,
\end{aligned} \tag{35a,b}$$

$$\tau_{\beta 3}=\frac{x_\beta}{2\pi r}\int\limits_0^\infty \frac{\overline{p}}{\varphi(\xi)}\left(g_{21}e^{-x_3\xi}+g_{22}e^{-x_3\zeta}\right)\xi J_1(\xi r)\mathrm{d}\xi,$$

$$\tau_{12}=\frac{x_1x_2}{2\pi r^2}\int\limits_0^\infty \frac{\overline{p}}{\varphi(\xi)}\left(h_{11}e^{-x_3\xi}+h_{12}e^{-x_3\zeta}\right)\xi J_2(\xi r)\mathrm{d}\xi,$$

$$\tau_{33}=-\frac{1}{2\pi}\int\limits_0^\infty \frac{\overline{p}}{\varphi(\xi)}\left(g_{31}e^{-x_3\xi}+g_{32}e^{-x_3\zeta}\right)\xi J_0(\xi r)\mathrm{d}\xi,$$

$$\tau_{\beta\beta}=\frac{1}{4\pi}\int\limits_0^\infty \frac{\overline{p}}{\varphi(\xi)}\left\{\left[2g_{41}(\xi)+g_{42}(\xi)\xi^2\right]\xi J_0(\xi r)+\left(1-2x_\beta^2r^{-2}\right)g_{42}(\xi)\xi^3J_2(\xi r)\right\}\mathrm{d}\xi, \tag{36a-d}$$

where $r=(x_\alpha x_\alpha)^{1/2}$, J_n is the Bessel function of the first kind of order n (with $n=0,\ 1,\ 2$), $h_{11},h_{12},h_{21},h_{22},g_{21},g_{22},g_{31}$ and g_{32} are given in Eqs. (31a-d) and (32c-f), and g_{41},g_{42} are defined as

$$\begin{aligned}g_{41}(\xi)&=2\nu\left\{-\left[1-\nu+2l^4\xi^2\zeta\left(\zeta-|\xi|\right)\right]e^{-x_3|\xi|}+\xi^2l^2e^{-x_3\zeta}\right\},\\ g_{42}(\xi)&=\frac{1}{\xi^2}\left\{-\left[\left(1-\nu+2l^4\xi^2\zeta^2\right)\left(1-2\nu-|\xi|\,x_3\right)+2\left(2\nu+|\xi|\,x_3\right)l^4\zeta\,|\xi|^3\right]e^{-x_3|\xi|}\right.\\ &\quad\left.+2\left(1-\nu+l^2\xi^2\right)l^2\xi^2e^{-x_3\zeta}\right\}.\end{aligned} \tag{36e,f}$$

Note that in reaching Eqs. (35a,b) and (36a-d) use has been made of the following inverse Fourier transform results [53]:

$$\begin{aligned}F^{-1}[\overline{f}(\xi)]&=\frac{1}{2\pi}\int\limits_0^\infty\overline{f}(\xi)\xi J_0(\xi r)\mathrm{d}\xi,\\ F^{-1}[\overline{f}(\xi)\xi_\alpha]&=\frac{ix_\alpha}{2\pi r}\int\limits_0^\infty\overline{f}(\xi)\xi^2J_1(\xi r)\mathrm{d}\xi,\\ F^{-1}[\overline{f}(\xi)\xi_1\xi_2]&=-\frac{x_1x_2}{2\pi r^2}\int\limits_0^\infty\overline{f}(\xi)\xi^3J_2(\xi r)\mathrm{d}\xi,\\ F^{-1}[\overline{f}(\xi)\xi_\alpha^2]&=\frac{1}{4\pi}\int\limits_0^\infty\overline{f}(\xi)\xi^3\left[J_0(\xi r)-\left(2x_\alpha^2r^{-2}-1\right)J_2(\xi r)\right]\mathrm{d}\xi,\end{aligned} \tag{37}$$

where F^{-1} denotes the inverse Fourier transform.

On the loading surface, Eqs. (35a,b) and (36a-d) give

$$\begin{aligned}u_\beta|_{x_3=0}&=-\frac{x_\beta}{4\pi\mu r}\int\limits_0^\infty\frac{\overline{p}}{\varphi(\xi)}\left[(1-\nu)(1-2\nu)-2\nu l^4\xi^2(\zeta-\xi)^2\right]J_1(\xi r)\mathrm{d}\xi,\\ u_3|_{x_3=0}&=\frac{1-\nu}{2\pi\mu}\int\limits_0^\infty\frac{\overline{p}}{\varphi(\xi)}\left[1-\nu-l^2\xi^3\zeta^{-1}+2l^4\xi^2\zeta(\zeta-\xi)\right]J_0(\xi r)\mathrm{d}\xi,\end{aligned} \tag{38a,b}$$

$$\tau_{\beta 3}|_{x_3=0} = -\frac{(1-\nu)x_\beta}{2\pi r}\int_0^\infty \frac{\overline{p}}{\zeta\varphi(\xi)}\xi^2 J_1(\xi r)\mathrm{d}\xi,$$

$$\tau_{12}|_{x_3=0} = \frac{x_1 x_2}{2\pi r^2}\int_0^\infty \frac{\overline{p}}{\varphi(\xi)}\left[(1-\nu)(1-2\nu) - 2\nu l^4\xi^2(\zeta-\xi)^2\right]\xi J_2(\xi r)\mathrm{d}\xi,$$

$$\tau_{33}|_{x_3=0} = -\frac{1}{2\pi}\int_0^\infty \frac{\overline{p}}{\varphi(\xi)}\left[1-\nu+2l^4\xi^2(\zeta-\xi)^2\right]\xi J_0(\xi r)\mathrm{d}\xi, \tag{39a-d}$$

$$\tau_{\beta\beta}|_{x_3=0} = \frac{1}{4\pi}\int_0^\infty \frac{\overline{p}}{\varphi(\xi)}\left\{\left[-(1-\nu)(1+2\nu) - 2\nu\left(2l^4\xi^4 - 2l^4\zeta|\xi|^3 + l^2\xi^2\right)\right]\xi J_0(\xi r)\right.$$
$$\left. + \left(1-2x_\beta^2 r^{-2}\right)\left[-(1-\nu)(1-2\nu) + 2\nu l^2\xi^2\left(1+2l^2\xi^2 - 2l^2\zeta|\xi|\right)\right]\xi J_2(\xi r)\right\}\mathrm{d}\xi.$$

It is observed from Eqs. (33a,b), (34a-d), (38a,b) and (39a-d) that, with $\varphi(\xi) \geq 1-\nu$ (see Eq. (28e)), the SSGET-based solutions predict smaller in-plane displacements $u_\alpha|_{x_3=0}$ and the Cauchy stress components $\tau_{\beta\beta}|_{x_3=0}$ than those predicted by the classical elasticity-based solution (with $l=0$). Also, the shear stress components τ_{13} and τ_{23} are no longer vanishing on the loading surface $x_3=0$ when the strain gradient effect is considered (with $l \neq 0$). These observations will be quantitatively shown in the next section.

5. Specific solutions

The general solutions for the half-space and half-plane problems derived in Sect. 4 are expressed in integral forms. These integrals are specified or evaluated in this section for several simple shapes of loading $p(r)$ (including a concentrated force and a uniform pressure distribution) to obtain specific solutions, which are compared to the counterpart solutions based on classical elasticity to illustrate the differences.

5.1. Concentrated force

The problem of an elastic half-space loaded by a concentrated force is known as the Boussinesq problem, while the problem of an elastic half-plane loaded by a concentrated force is called the Flamant problem (e.g., [3,28,40]).

For the Flamant problem, $p(r) = P\delta(x_1)$ and thus $\overline{p} = P$ in the Fourier domain. It then follows from Eqs. (33a,b) and (34a-d) that the current SSGET-based solution yields the surface displacements as

$$u_1|_{x_3=0} = -\frac{P}{2\pi\mu}\int_0^\infty \frac{1}{\xi\varphi(\xi)}\left[(1-\nu)(1-2\nu) - 2\nu l^4\xi^2(\zeta-\xi)^2\right]\sin(\xi x_1)\mathrm{d}\xi,$$
$$u_3|_{x_3=0} = \frac{(1-\nu)P}{\pi\mu}\int_0^\infty \frac{1}{\xi\varphi(\xi)}\left[1-\nu-l^2\xi^3\zeta^{-1} - 2l^4\xi^2\zeta(\xi-\zeta)\right]\cos(\xi x_1)\mathrm{d}\xi, \tag{40a,b}$$

and the surface Cauchy stress components as

$$\begin{aligned}
\tau_{11}|_{x_3=0} &= -\frac{(1-\nu)P}{\pi}\int_0^\infty \frac{1}{\varphi(\xi)}\cos(\xi x_1)\mathrm{d}\xi,\\
\tau_{13}|_{x_3=0} &= -\frac{(1-\nu)P}{\pi}\int_0^\infty \frac{\xi}{\zeta\varphi(\xi)}\sin(\xi x_1)\mathrm{d}\xi,\\
\tau_{33}|_{x_3=0} &= -\frac{P}{\pi}\int_0^\infty \frac{1}{\varphi(\xi)}\left[1-\nu+2l^4\xi^2(\zeta-\xi)^2\right]\cos(\xi x_1)\mathrm{d}\xi,\\
\tau_{22}|_{x_3=0} &= -\frac{2\nu P}{\pi}\int_0^\infty \frac{1}{\varphi(\xi)}\left[1-\nu+2l^4\xi^3(\xi-\zeta)+l^2\xi^2\right]\cos(\xi x_1)\mathrm{d}\xi.
\end{aligned} \tag{41a-d}$$

For the Boussinesq problem, $p(r)=P\delta(x_1)\delta(x_2)$ and thus $\overline{p}=P$ in the Fourier domain. Then, the current SSGET-based solution gives from Eqs. (38a,b) and (39a-d) that the surface displacements as

$$\begin{aligned}
u_\beta|_{x_3=0} &= -\frac{Px_\beta}{4\pi\mu r}\int_0^\infty \frac{1}{\varphi(\xi)}\left[(1-\nu)(1-2\nu)-2\nu l^4\xi^2(\zeta-\xi)^2\right]J_1(\xi r)\mathrm{d}\xi,\\
u_3|_{x_3=0} &= \frac{(1-\nu)P}{2\pi\mu}\int_0^\infty \frac{1}{\varphi(\xi)}\left[1-\nu-l^2\xi^3\zeta^{-1}+2l^4\xi^2\zeta(\zeta-\xi)\right]J_0(\xi r)\mathrm{d}\xi,
\end{aligned} \tag{42a,b}$$

and the surface Cauchy stress components as

$$\begin{aligned}
\tau_{\beta 3}|_{x_3=0} &= -\frac{(1-\nu)Px_\beta}{2\pi r}\int_0^\infty \frac{\xi^2 J_1(\xi r)}{\zeta\varphi(\xi)}\mathrm{d}\xi,\\
\tau_{12}|_{x_3=0} &= \frac{Px_1x_2}{2\pi r^2}\int_0^\infty \frac{\xi J_2(\xi r)}{\varphi(\xi)}\left[(1-\nu)(1-2\nu)-2\nu l^4\xi^2(\zeta-\xi)^2\right]\mathrm{d}\xi,\\
\tau_{\beta\beta}|_{x_3=0} &= \frac{P}{4\pi}\int_0^\infty \frac{1}{\varphi(\xi)}\left\{\left[-(1-\nu)(1+2\nu)-2\nu\left(2l^4\xi^4-2l^4\zeta|\xi|^3+l^2\xi^2\right)\right]\xi J_0(\xi r)\right.\\
&\quad\left.+\left(1-2x_\beta^2r^{-2}\right)\left[-(1-\nu)(1-2\nu)+2\nu l^2\xi^2\left(1+2l^2\xi^2-2l^2\zeta|\xi|\right)\right]\xi J_2(\xi r)\right\}\mathrm{d}\xi,\\
\tau_{33}|_{x_3=0} &= -\frac{P}{2\pi}\int_0^\infty \frac{\xi J_0(\xi r)}{\varphi(\xi)}\left[1-\nu+2l^4\xi^2(\zeta-\xi)^2\right]\mathrm{d}\xi.
\end{aligned} \tag{43a-d}$$

The classical elasticity-based Flamant and Boussinesq solutions can be recovered from the current SSGET-based solutions as special cases. Setting $l=0$ and $\overline{p}=P$ in Eqs. (30a-c) yields, along with Eqs. (28e) and (32a-f),

$$\tau_{11}^{\mathrm{c}}=-\frac{2P}{\pi}\frac{x_3x_1^2}{r^4},\tau_{13}^{\mathrm{c}}=-\frac{2P}{\pi}\frac{x_1x_3^2}{r^4},\tau_{33}^{\mathrm{c}}=-\frac{2P}{\pi}\frac{x_3^3}{r^4}, \tag{44a-c}$$

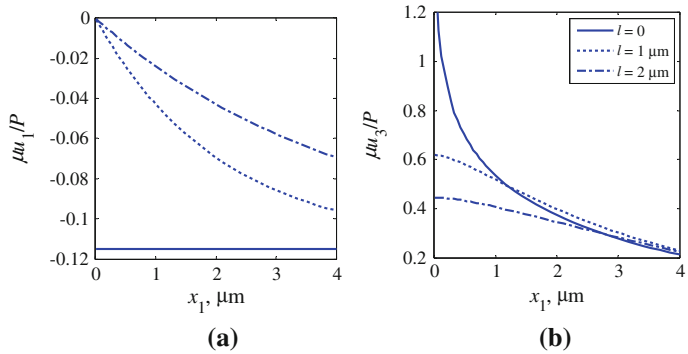

FIG. 2. Surface displacements of a half-plane loaded by a concentrated normal force P at $(x_1, x_3) = (0, 0)$. The legend in the *box* also applies to (**a**)

which are the same as those in the classical Flamant solution (e.g., [28,40]). In reaching Eqs. (44a-c), use has been made of the following results:

$$\int_0^\infty e^{-at}\sin(bt)\mathrm{d}t = \frac{b}{a^2+b^2}, \int_0^\infty e^{-at}\cos(bt)\mathrm{d}t = \frac{a}{a^2+b^2},$$
$$\int_0^\infty te^{-at}\sin(bt)\mathrm{d}t = \frac{2ab}{(a^2+b^2)^2}, \int_0^\infty te^{-at}\cos(bt)\mathrm{d}t = \frac{a^2-b^2}{(a^2+b^2)^2}, \tag{45a-d}$$

which hold for any $a\,(>0)$ and b.

Similarly, letting $l = 0$ and $\bar{p} = P$ in Eqs. (36a,c) gives, together with Eqs. (28e) and (32c-f),

$$\tau_{\beta 3} = -\frac{P}{2\pi}\frac{3x_3^2 x_\beta}{(r^2+x_3^2)^{5/2}}, \tau_{33} = -\frac{3P}{2\pi}\frac{x_3^3}{(r^2+x_3^2)^{5/2}}, \tag{46a,b}$$

which are the same as those in the classical Boussinesq solution (e.g., [28]). In obtaining Eqs. (46a,b), the following results have been used:

$$\int_0^\infty \xi e^{-x_3\xi}J_0(\xi r)\mathrm{d}\xi = \frac{x_3}{(r^2+x_3^2)^{3/2}}, \quad \int_0^\infty \xi^2 e^{-x_3\xi}J_0(\xi r)\mathrm{d}\xi = \frac{2x_3^2-r^2}{(r^2+x_3^2)^{5/2}},$$
$$\int_0^\infty \xi^2 e^{-x_3\xi}J_1(\xi r)\mathrm{d}\xi = \frac{3rx_3}{(r^2+x_3^2)^{5/2}}. \tag{47a-c}$$

According to the classical Flamant solution, the in-plane displacement u_1 is discontinuous and the out-of-plane displacement u_3 is unbounded at the point of force application (e.g., [40]). However, such discontinuity and singularity are not exhibited by the SSGET-based solution of the same problem. The numerical results depicted in Fig. 2 show that at the loading point $(x_1, x_3) = (0, 0)$, $u_1|_{x_3=0}$ vanishes (and thus is continuous) and $u_3|_{x_3=0}$ is well defined for each case with $l \neq 0$ (when the SSGET-based solution is used). Similar observations were made in [18] based on their solution. Such mechanical responses are more physical than the discontinuous and singular behaviors predicted by the classical solution. In addition, the current SSGET-based solution (with $l \neq 0$) deviates significantly from the classical one (with $l = 0$) in the vicinity of the loading point, even though it converges to the latter at a far distance (with x_1 becoming sufficiently large). Also, the discrepancy between the current solution and the classical one decreases as the material parameter l decreases.

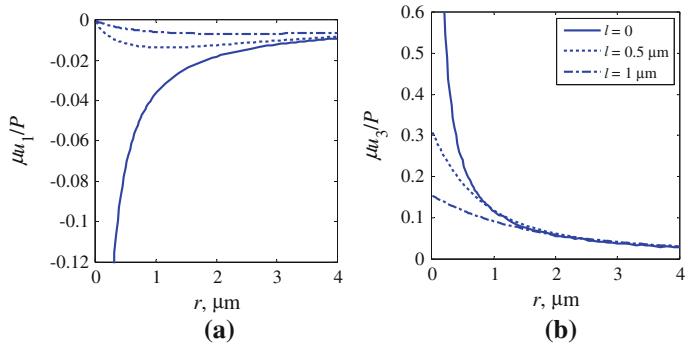

FIG. 3. Surface displacements along $x_2 = 0$ of a half-space loaded by a concentrated normal force P at $(x_1, x_2, x_3) = (0, 0, 0)$. The legend in the *box* also applies to (**a**)

Similar trends are observed for the SSGET-based solution of the Boussinesq problem, as shown in Fig. 3.

5.2. Uniformly distributed normal force

For a uniformly distributed normal force of intensity q_0 applied on the interval $-a < x_1 < a$ on the surface of a half-plane, Eq. (19a) gives

$$\overline{p} = 2q_0\xi^{-1}\sin(\xi a). \tag{48}$$

For a half-space, if the uniformly distributed normal force of intensity q_0 is applied over the region $r < a$, then it follows from Eq. (20a) that

$$\overline{p} = 2\pi a q_0\xi^{-1}J_1(a\xi). \tag{49}$$

Using Eq. (48) in Eqs. (29a-c) and (30a-d) gives the solution for the half-plane problem as

$$\begin{aligned}
u_1 &= -\frac{q_0}{\pi\mu}\int_0^\infty \frac{1}{\xi^2\varphi(\xi)}\left(h_{11}e^{-x_3\xi} + h_{12}e^{-x_3\zeta}\right)\sin(\xi a)\sin(\xi x_1)\mathrm{d}\xi,\\
u_2 &= 0,\\
u_3 &= \frac{q_0}{\pi\mu}\int_0^\infty \frac{1}{\xi^2\varphi(\xi)}\left(h_{21}e^{-x_3\xi} + h_{22}e^{-x_3\zeta}\right)\sin(\xi a)\cos(\xi x_1)\mathrm{d}\xi,\\
\tau_{11} &= -\frac{2q_0}{\pi}\int_0^\infty \frac{1}{\xi\varphi(\xi)}\left(g_{11}e^{-x_3\xi} + g_{12}e^{-x_3\zeta}\right)\sin(\xi a)\cos(\xi x_1)\mathrm{d}\xi,\\
\tau_{13} &= \frac{2q_0}{\pi}\int_0^\infty \frac{1}{\xi\varphi(\xi)}\left(g_{21}e^{-x_3\xi} + g_{22}e^{-x_3\zeta}\right)\sin(\xi a)\sin(\xi x_1)\mathrm{d}\xi,\\
\tau_{33} &= -\frac{2q_0}{\pi}\int_0^\infty \frac{1}{\xi\varphi(\xi)}\left(g_{31}e^{-x_3\xi} + g_{32}e^{-x_3\zeta}\right)\sin(\xi a)\cos(\xi x_1)\mathrm{d}\xi,\\
\tau_{22} &= -\frac{2\nu q_0}{\pi}\int_0^\infty \frac{1}{\xi\varphi(\xi)}\left[(g_{11}+g_{31})e^{-x_3\xi} + (g_{12}+g_{32})e^{-x_3\zeta}\right]\sin(\xi a)\cos(\xi x_1)\mathrm{d}\xi.
\end{aligned} \tag{50a-g}$$

Similarly, substituting Eq. (49) into Eqs. (35a,b) and (36a-d)) yields the solution for the half-space problem as

$$
\begin{aligned}
u_\beta &= -\frac{aq_0x_\beta}{2\mu r}\int_0^\infty \frac{1}{\xi\varphi(\xi)}\left(h_{11}e^{-x_3\xi}+h_{12}e^{-x_3\zeta}\right)J_1(a\xi)J_1(\xi r)\mathrm{d}\xi,\\
u_3 &= \frac{aq_0}{2\mu}\int_0^\infty \frac{1}{\xi\varphi(\xi)}\left(h_{21}e^{-x_3\xi}+h_{22}e^{-x_3\zeta}\right)J_0(\xi r)J_1(a\xi)\mathrm{d}\xi,\\
\tau_{\beta 3} &= \frac{aq_0x_\beta}{r}\int_0^\infty \frac{1}{\varphi(\xi)}\left(g_{21}e^{-x_3\xi}+g_{22}e^{-x_3\zeta}\right)J_1(a\xi)J_1(\xi r)\mathrm{d}\xi,\\
\tau_{12} &= \frac{aq_0x_1x_2}{r^2}\int_0^\infty \frac{1}{\varphi(\xi)}\left(h_{11}e^{-x_3\xi}+h_{12}e^{-x_3\zeta}\right)J_1(a\xi)J_2(\xi r)\mathrm{d}\xi,\\
\tau_{\beta\beta} &= \frac{aq_0}{2}\int_0^\infty \frac{1}{\varphi(\xi)}\left\{\left[2g_{41}(\xi)+g_{42}(\xi)\xi^2\right]J_0(\xi r)+\left(1-2x_\beta^2r^{-2}\right)g_{42}(\xi)\xi^2J_2(\xi r)\right\}J_1(a\xi)\mathrm{d}\xi,\\
\tau_{33} &= -aq_0\int_0^\infty \frac{1}{\varphi(\xi)}\left(g_{31}e^{-x_3\xi}+g_{32}e^{-x_3\zeta}\right)J_0(\xi r)J_1(a\xi)\mathrm{d}\xi.
\end{aligned}
\tag{51a-f}
$$

The numerical results displayed in Figs. 4 and 5 show that $u_1|_{x_3=0}$ and $\tau_{33}|_{x_3=0}$ given by the SSGET-based solutions for the half-plane and half-space problems change smoothly across the loading periphery, unlike those given by the classical elasticity-based solutions (with $l=0$), which exhibit sharp angles. A similar observation was made for the near-tip displacement in 2-D crack problems (e.g., [17,42]), which varies more smoothly if a strain gradient elasticity theory is used to describe the material behavior.

6. Indentation

The problem of an elastic solid indented by a punch is of practical interest. Classical elasticity cannot explain the size effect on elastic properties observed at the micron and nanometer scales (e.g., [2,7,45]) due to a lack of any material length scale parameter.

The indentation size effect is studied herein using the newly derived SSGET-based solution for the half-space contact problem that contains a material length scale parameter. Three indenter shapes (or punch profiles), i.e., flat-ended, spherical and conical, are considered, as was done in [6,53].

6.1. Flat-ended punch

The problem of an elastic half-space indented by a rigid flat-ended cylindrical punch was first solved in [5] using the classical theory of elasticity. According to his solution, the pressure profile under the punch takes the form (e.g., [3]):

$$
p_B(r) = \frac{P}{2\pi a}(a^2-r^2)^{-1/2}, \tag{52}
$$

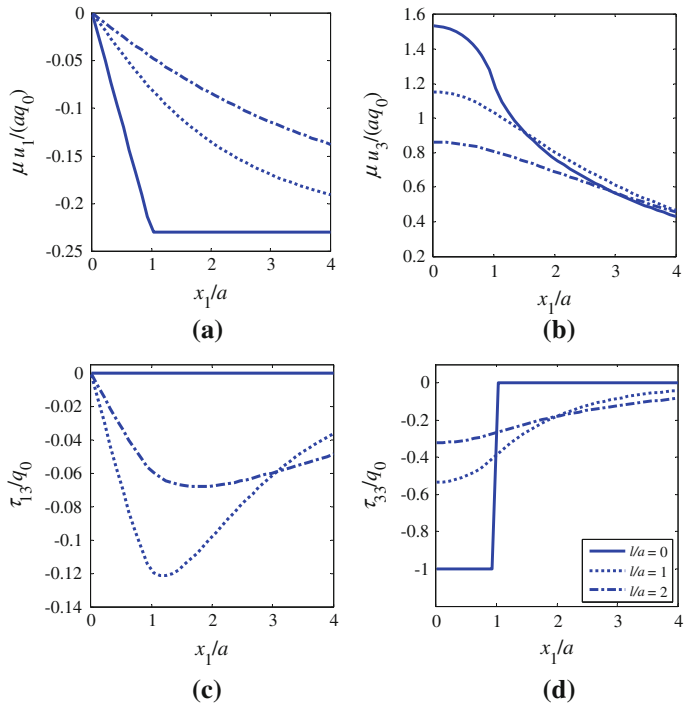

FIG. 4. Surface displacements and Cauchy stress components of a half-plane subjected to a uniform pressure q_0 on $-a < x_1 < a$. The legend in the *box* also applies to (**a**), (**b**) and (**c**)

where a is the radius of the cylindrical punch, and P is the total load applied on the punch. That is,

$$P = 2\pi \int_0^a p_B(r) r \mathrm{d}r. \tag{53}$$

Taking Fourier transforms (see Eq. (20a)) on Eq. (52) gives

$$\overline{p}_B(\xi) = \frac{P}{a\xi} \sin(a\xi). \tag{54}$$

The displacement and stress components can then be readily obtained by using Eq. (54) in the general solution given in Eqs. (35a,b) and (36a-d) for the half-space problem. In particular, substituting Eq. (54) into Eq. (35b) yields, along with Eqs. (31c,d), the indentation depth (defined as the depth of penetration of the punch tip) δ_B as

$$\delta_B = u_3|_{r=0,x_3=0} = \frac{P(1-\nu)}{2\pi a\mu} \int_0^\infty \frac{\phi(\xi)}{\xi\varphi(\xi)} \sin(a\xi)\mathrm{d}\xi, \tag{55a}$$

where

$$\phi(\xi) = 1 - \nu - l^2\xi^3\zeta^{-1} + 2l^4\xi^2\zeta(\zeta - \xi), \tag{55b}$$

and $\varphi(\xi)$ is defined in Eq. (28e).

The displacement and Cauchy stress components on the surface $x_3 = 0$ of the half-space at different values of l/a are shown in Fig. 6, where the corresponding components given by the classical solution (with $l = 0$) are also displayed for comparison. The numerical values shown in Fig. 6 are obtained by

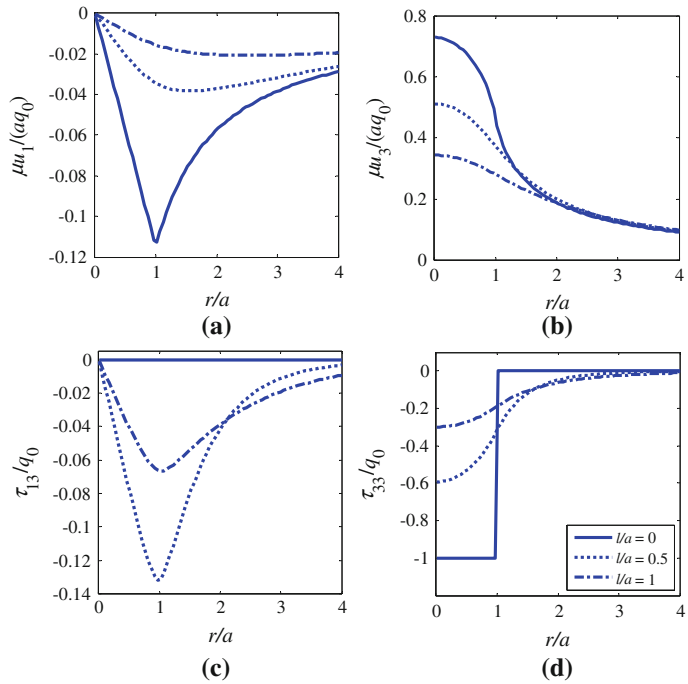

FIG. 5. Surface displacements and Cauchy stress components along $x_2 = 0$ of a half-space subjected to a uniform pressure q_0 in the region $r < a$. The legend in the *box* also applies to (**a**), (**b**) and (**c**)

using Eq. (54) in Eqs. (38a,b) and (39a,c). It is seen that the current SSGET-based solution predicts considerably smaller surface displacements than the classical solution inside and near the loading zone. In addition, the Cauchy stress components on the surface $\tau_{13}|_{x_3=0}$ and $\tau_{33}|_{x_3=0}$ given by the current solution are well defined and smooth.

6.2. Spherical punch

The Hertz's solution [20] for the frictionless and non-adhesive contact of two elastic spheres is the earliest one in contact mechanics. According to Hertz's solution, the pressure distribution under the spherical indenter has the form (e.g., [3]):

$$p_H(r) = \frac{3P}{2\pi a^3}\sqrt{a^2 - r^2}, \tag{56}$$

where a is the radius of the contact zone, and P is the total axial force applied on the punch. Taking Fourier transforms (see Eq. (20a)) on Eq. (56) yields

$$\overline{p}_H(\xi) = \frac{3P}{\xi^3 a^3}\left[\sin(a\xi) - a\xi\cos(a\xi)\right]. \tag{57}$$

The displacement and stress components can then be readily obtained by using Eq. (57) in the general solution given in Eqs. (35a,b) and (36a-d). In particular, using Eq. (57) in Eq. (35b) gives the indentation depth δ_H as

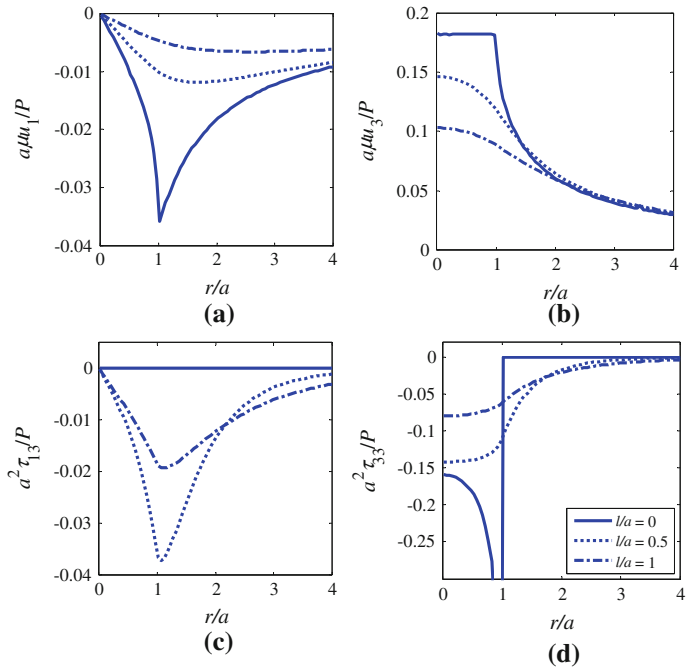

FIG. 6. Variations of the surface displacements and Cauchy stress components along $x_2 = 0$ in a half-space with the Boussinesq pressure distribution. The legend in the *box* also applies to (**a**), (**b**) and (**c**)

$$\delta_H = u_3|_{r=0,x_3=0} = \frac{3P(1-\nu)}{2\pi a^3 \mu} \int_0^\infty \frac{a^2 \phi(\frac{t}{a})}{t^3 \varphi(\frac{t}{a})} (\sin t - t\cos t)\, \mathrm{d}t, \tag{58}$$

where ϕ and φ are defined in Eq. (55b) and Eq. (28e), respectively.

Figure 7 shows the displacement and Cauchy stress components on the surface $x_3 = 0$ of the half-space at different values of l/a, where the corresponding components given by the classical solution (with $l = 0$) are also displayed for comparison. The numerical values shown in Fig. 7 are obtained by using Eq. (57) in Eqs. (38a,b) and (39a,c). It is observed from Fig. 7 that the surface displacements predicted by the current SSGET-based solution are significantly smaller than those by the classical solution both inside and near the loading zone. Also, $u_1|_{x_3=0}$ and $\tau_{33}|_{x_3=0}$ given by the current solution are smoother. These microstructural effects (as measured by the material length scale parameter l) on the elastic field are similar to those observed earlier for the flat-ended punch problem.

6.3. Conical punch

Conical indenters are frequently used in indentation tests. For a cone-shaped punch subjected to the axial load P, the pressure distribution in the contact zone has the form (e.g., [44])

$$p_C(r) = \frac{P}{\pi a^2} \cosh^{-1} \frac{a}{r}. \tag{59}$$

Taking Fourier transforms (see Eq. (20a)) on Eq. (59) gives

$$\overline{p}_C(\xi) = \frac{2P}{a^2 \xi^2} \left[1 - \cos(\xi a)\right]. \tag{60}$$

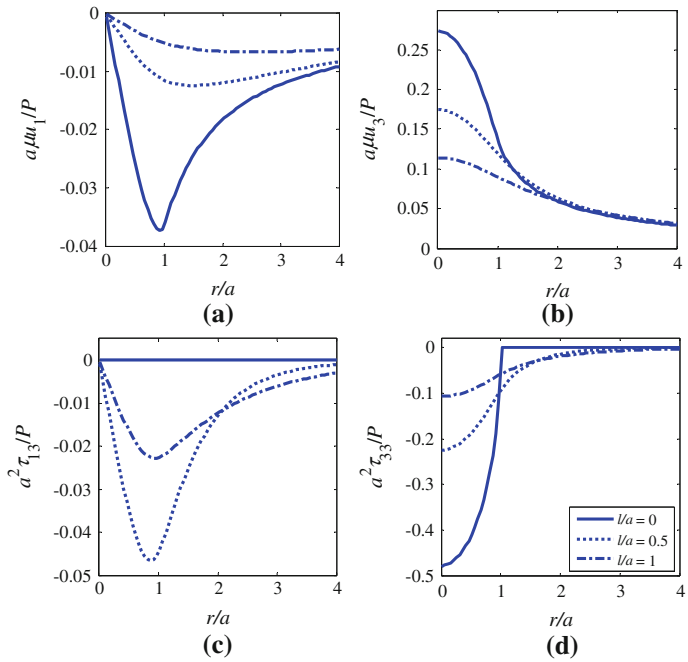

FIG. 7. Variations of the surface displacements and Cauchy stress components along $x_2 = 0$ in a half-space with the Hertzian pressure distribution. The legend in the *box* also applies to (**a**), (**b**) and (**c**)

The displacement and stress components can then be readily obtained by using Eq. (60) in the general solution given in Eqs. (35a,b) and (36a-d). In particular, substituting Eq. (60) into Eq. (35b) yields the indentation depth δ_C as

$$\delta_C = u_3|_{r=0,x_3=0} = \frac{P(1-\nu)}{\pi a^2 \mu} \int_0^\infty \frac{a\phi(\frac{t}{a})}{t^2 \varphi(\frac{t}{a})} (1 - \cos t)\, \mathrm{d}t, \tag{61}$$

where ϕ and φ are defined in Eq. (55b) and Eq. (28e), respectively.

Figure 8 displays the displacement and Cauchy stress components on the surface $x_3 = 0$ of the half-space at different values of l/a, where the corresponding components given by the classical solution (with $l = 0$) are also shown for comparison. The numerical results in Fig. 8 are obtained by using Eq. (60) in Eqs. (38a,b) and (39a,c). Microstructural effects (through l) on the elastic field similar to those observed for the flat-ended and spherical punch problems based on Figs. 6 and 7 are shown in Fig. 8.

6.4. Depth-dependent hardness

Consider the indentation hardness defined by (e.g., [49,53])

$$H = \frac{P}{\delta}, \tag{62}$$

where P and δ are, respectively, the total applied load and indentation depth.

When the strain gradient effect is ignored, $l = 0$ and thus $\varphi(\xi) = 1 - \nu = \phi(\xi)$ according to Eqs. (28e) and (55b). It then follows from Eqs. (62), (55a), (58) and (61) that

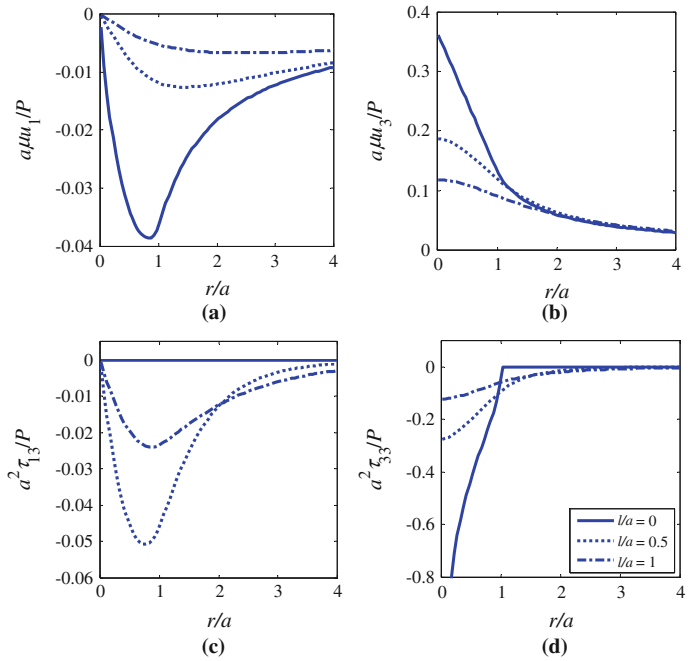

FIG. 8. Variations of the surface displacements and Cauchy stress components along $x_2 = 0$ in a half-space with the conical punch pressure distribution. The legend in the *box* also applies to (**a**), (**b**) and (**c**)

$$H_B^c = \frac{4\mu a}{1-\nu}, \quad H_H^c = \frac{8\mu a}{3(1-\nu)}, \quad H_C^c = \frac{2\mu a}{1-\nu} \tag{63}$$

as the indentation hardness for the three punch profiles based on classical elasticity.

When the strain gradient effect is considered, the indentation hardness can be obtained from Eqs. (62), (55a), (58), (61) and (63) as

$$\frac{H_B^c}{H_B} = 1 - \frac{2}{\pi}\int_0^\infty \psi(a,t)t^{-1}\sin t\mathrm{d}t \tag{64a}$$

for the Boussinesq flat-ended cylindrical punch,

$$\frac{H_H^c}{H_H} = 1 - \frac{4}{\pi}\int_0^\infty \psi(a,t)t^{-3}\left(\sin t - t\cos t\right)\mathrm{d}t \tag{64b}$$

for the Hertzian spherical punch, and

$$\frac{H_C^c}{H_C} = 1 - \frac{2}{\pi}\int_0^\infty \psi(a,t)t^{-2}\left(1-\cos t\right)\mathrm{d}t \tag{64c}$$

for the conical punch, where

$$\psi(a,t) = 1 - \frac{\phi(\frac{t}{a})}{\varphi(\frac{t}{a})} = \tilde{l}^2t^2\frac{2(1-\nu)+t\tilde{\zeta}^{-1}-2\tilde{l}^4t\tilde{\zeta}(\tilde{\zeta}-t)^2}{(1-\nu)(1+2\tilde{l}^2t^2)+2\tilde{l}^6\tilde{\zeta}^2t^2(\tilde{\zeta}-t)^2}, \tag{65}$$

with $\tilde{l} = l/a$ and $\tilde{\zeta} = \sqrt{t^2+\frac{1}{\tilde{l}^2}}$.

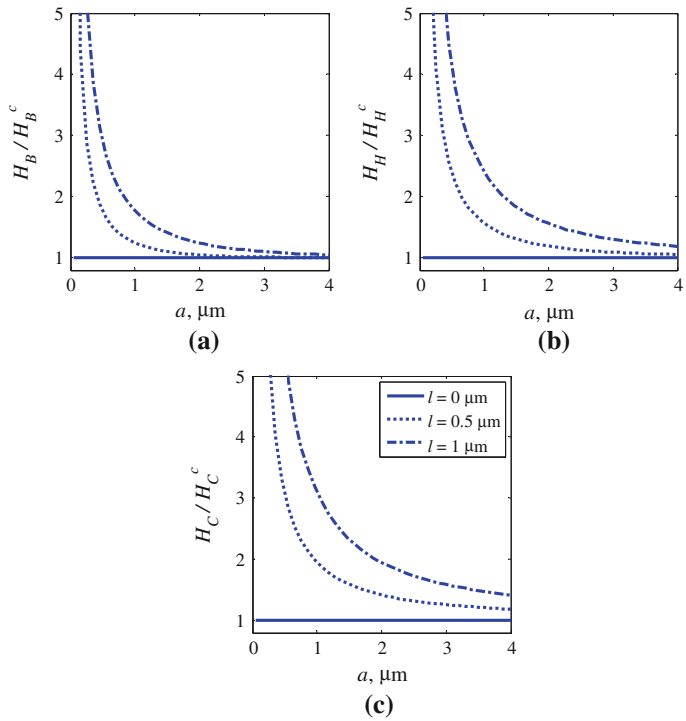

FIG. 9. Indentation hardness changing with the contact radius at different l values: (**a**) flat-ended punch, (**b**) spherical punch, and (**c**) conical punch

Clearly, when $l = 0, \psi(a, t) = 0$ from Eq. (65). It then follows from Eqs. (64a-c) that $H_B = H_B^c$, $H_H = H_H^c$, and $H_C = H_C^c$. That is, when the strain gradient effect is not considered, the indentation hardness given by the current SSGET-based solution reduces to that given by the classical elasticity-based solution in each of the three cases. Also, for macro-indentation tests with $\tilde{l} = l/a \ll 1, \psi(a, t) \to 0$ from Eq. (65), and the current solution converges to the classical one, giving $H_B = H_B^c$, $H_H = H_H^c$, and $H_C = H_C^c$. However, for micro-indentation tests, the size effect can be significant. As illustrated in Fig. 9, the indentation hardness predicted by the current solution is considerably higher than that given by the classical solution.

Figure 9 shows variations of the indentation hardness with the contact zone radius a at different values of l/a. For each of the three punch profiles considered, it is seen from Fig. 9 that the indentation hardness increases with decreasing a and increasing l. The punch profile is also observed to have an influence on the indentation hardness, as displayed in Fig. 10. For given values of l and a, the indentation hardness measured by a conical punch is seen to be the largest and that by a flat-ended cylindrical punch to be the smallest. By contrast, the indentation hardness predicted by the classical elasticity-based solution is a constant (independent of the indenter size (reflected through a) and the material microstructure (measured by l)) for each punch profile, as shown in Fig. 9.

7. Summary

The contact problems of a half-plane and a half-space, respectively, subjected to a symmetrically distributed normal force of arbitrary profile are solved using a simplified strain gradient elasticity theory

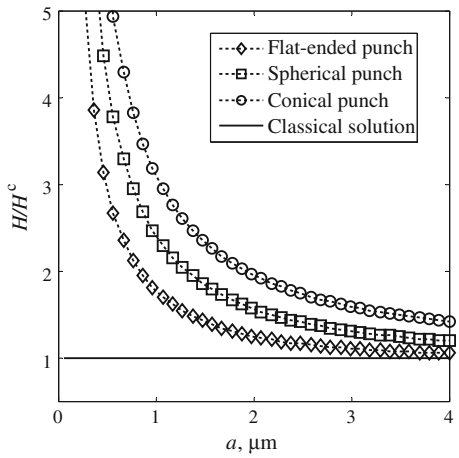

FIG. 10. Indentation hardness for different punch profiles (with $l = 1\mu m$)

(SSGET). The general SSGET-based solutions for the half-plane and half-space problems are derived in a unified manner using Mindlin's potential function method and Fourier transforms. The current solutions contain one material length scale parameter and can capture the indentation size effect at small length scales. The classical elasticity-based solutions of the half-plane and half-space problems are recovered as special cases when the strain gradient effect is not considered. The general solution for the half-space problem is also applied to analyze the indentation of an elastic half-space by a flat-ended cylindrical punch, a spherical punch, and a conical punch, respectively.

The numerical results show that the displacement discontinuity and/or singularity exhibited by the classical solutions of the Flamant and Boussinesq problems are not displayed by the current SSGET-based solutions. The displacement and Cauchy stress components on the loading surface predicted by the newly derived solutions are found to deviate considerably from those given by the classical solutions inside and near the loading zone. The SSGET-based solutions converge to the classical solutions at a distance away from the loading zone. The discrepancy between the two sets of solutions increases as the material length scale parameter becomes larger. The indentation hardness given by the current SSGET-based half-space problem solution is significantly higher than that provided by the classical elasticity-based solution when the indentation radius is small.

Acknowledgements

The work reported here has been funded by two grants from the U.S. National Science Foundation (NSF), with Drs. Clark V. Cooper and Martin L. Dunn as the program directors. This support is gratefully acknowledged.

References

1. Altan, B.S., Aifantis, E.C.: On some aspects in the special theory of gradient elasticity. J. Mech. Behav. Mater. **8**(3), 231–282 (1997)
2. Arinstein, A., Burman, M., Gendelman, O., Zussman, E.: Effect of supramolecular structure on polymer nanofibre elasticity. Nat. Nanotechnol. **2**, 59–62 (2007)
3. Barber, J.R.: Elasticity, 2nd edn. Kluwer, Dordrecht (2002)

4. Barbot, S., Fialko, Y.: Fourier-domain Green's function for an elastic semi-infinite solid under gravity, with applications to earthquake and volcano deformation. Geophys. J. Int. **182**, 568–582 (2010)
5. Boussinesq, J.: Application des potentiels à l'étude de l'équilibre et du mouvement des solides élastiques. Gauthiers-Villars, Paris (1885)
6. Chen, W.Q., Pan, E.N., Wang, H.M., Zhang, C.Z.: Theory of indentation on multiferroic composite materials. J. Mech. Phys. Solids **58**, 1524–1551 (2010)
7. Cho, J., Joshi, M.S., Sun, C.T.: Effect of inclusion size on mechanical properties of polymeric composites with micro and nano particles. Compos. Sci. Tech. **66**, 1941–1952 (2006)
8. Cosserat, E., Cosserat, F.: Théorie des Corps Déformables. A. Hermann et Fils, Paris (1909)
9. Dhaliwal, R.S.: The axisymmetric Boussinesq problem for a semi-space in couple-stress theory. Int. J. Eng. Sci. **11**, 1161–1174 (1973)
10. Gao, X.-L., Liu, M.Q.: Strain gradient solution for the Eshelby-type polyhedral inclusion problem. J. Mech. Phys. Solids **60**, 261–276 (2012)
11. Gao, X.-L., Ma, H.M.: Green's function and Eshelby's tensor based on a simplified strain gradient elasticity theory. Acta Mech. **207**, 163–181 (2009)
12. Gao, X.-L., Ma, H.M.: Solution of Eshelby's inclusion problem with a bounded domain and Eshelby's tensor for a spherical inclusion in a finite spherical matrix based on a simplified strain gradient elasticity theory. J. Mech. Phys. Solids **58**, 779–797 (2010)
13. Gao, X.-L., Ma, H.M.: Strain gradient solution for Eshelby's ellipsoidal inclusion problem. Proc. R. Soc. A **466**, 2425–2446 (2010)
14. Gao, X.-L., Ma, H.M.: Strain gradient solution for the Eshelby-type anti-plane strain inclusion problem. Acta Mech. **223**, 1067–1080 (2012)
15. Gao, X.-L., Park, S.K.: Variational formulation of a simplified strain gradient elasticity theory and its application to a pressurized thick-walled cylinder problem. Int. J. Solids Struct. **44**, 7486–7499 (2007)
16. Gao, X.-L., Park, S.K., Ma, H.M.: Analytical solution for a pressurized thick-walled spherical shell based on a simplified strain gradient elasticity theory. Math. Mech. Solids **14**, 747–758 (2009)
17. Georgiadis, H.G.: The mode-III crack problem in microstructured solids governed by dipolar gradient elasticity: static and dynamic analysis. ASME J. Appl. Mech. **70**, 517–530 (2003)
18. Georgiadis, H.G., Anagnostou, D.S.: Problems of the Flamant–Boussinesq and Kelvin type in dipolar gradient elasticity. J. Elast. **90**, 71–98 (2008)
19. Harding, J.W., Sneddon, I.N.: The elastic stresses produced by the indentation of the plane surface of a semi-infinite elastic solid by a rigid punch. Proc. Cambridge Philos. Soc. **41**, 16–26 (1945)
20. Hertz, H.: Über die Berührung fester elastischer Körper. J. Reine Angew. Math. **92**, 156–171 (1882)
21. Hutchinson, J.W.: Plasticity at the micron scale. Int. J. Solids Struct. **37**, 225–238 (2000)
22. Karlis, G.F., Charalambopoulos, A., Polyzos, D.: An advanced boundary element method for solving 2D and 3D static problems in Mindlin's strain-gradient theory of elasticity. Int J. Numer. Method Eng. **83**, 1407–1427 (2010)
23. Koiter, W.T.: Couple-stresses in the theory of elasticity, I & II. Proc. K. Ned. Akad. Wet. (B) **67**, 17–44 (1964)
24. Lakes, R.: Experimental methods for study of Cosserat elastic solids and other generalized elastic continua. In: Mühlhaus, H. (ed.) Continuum models for materials with micro-structure, pp. 1–22. Wiley, New York (1995)
25. Lazar, M.: The fundamentals of non-singular dislocations in the theory of gradient elasticity: dislocation loops and straight dislocations. Int. J. Solids Struct. (2012). doi:10.1016/j.ijsolstr.2012.09.017
26. Lazar, M., Maugin, G.A.: Nonsingular stress and strain fields of dislocations and disclinations in first strain gradient elasticity. Int. J. Eng. Sci. **43**, 1157–1184 (2005)
27. Li, S., Miskioglu, I., Altan, B.S.: Solution to line loading of a semi-infinite solid in gradient elasticity. Int. J. Solids Struct. **41**, 3395–3410 (2004)
28. Little, R.W.: Elasticity. Prentice-Hall, Englewood Cliffs (1973)
29. Liu M.Q., Gao X.-L.: Strain gradient solution for the Eshelby-type polygonal inclusion problem. Int. J. Solids Struct. (2012). doi:10.1016/j.ijsolstr.2012.09.010
30. Ma, H.M., Gao, X.-L.: Eshelby's tensors for plane strain and cylindrical inclusions based on a simplified strain gradient elasticity theory. Acta Mech. **211**, 115–129 (2010)
31. Ma, H.M., Gao, X.-L.: Strain gradient solution for a finite-domain Eshelby-type plane strain inclusion problem and Eshelby's tensor for a cylindrical inclusion in a finite elastic matrix. Int. J. Solids Struct. **48**, 44–55 (2011)
32. Mindlin, R.D.: Influence of couple-stresses on stress concentrations. Exp. Mech. **3**, 1–7 (1963)
33. Mindlin, R.D.: Micro-structure in linear elasticity. Arch. Ration. Mech. Anal. **16**, 51–78 (1964)
34. Mindlin, R.D.: Second gradient of strain and surface-tension in linear elasticity. Int. J. Solids Struct. **1**, 417–438 (1965)
35. Mindlin, R.D., Eshel, N.N.: On first strain-gradient theories in linear elasticity. Int. J. Solids Struct. **4**, 109–124 (1968)
36. Mindlin, R.D., Tiersten, H.F.: Effects of couple-stresses in linear elasticity. Arch. Ration. Mech. Anal. **11**, 415–448 (1962)
37. Nix, W.D., Gao, H.: Indentation size effects in crystalline materials: a law for strain gradient plasticity. J. Mech. Phys. Solids **46**, 411–425 (1998)

38. Park, S.K., Gao, X.-L.: Variational formulation of a modified couple stress theory and its application to a simple shear problem. Z. Angew. Math. Phys. **59**, 904–917 (2008)
39. Polyzos, D., Tsepoura, K.G., Tsinopoulos, S.V., Beskos, D.E.: A boundary element method for solving 2-D and 3-D static gradient elastic problems. Part I. Integral formulation. Comput. Methods Appl. Mech. Eng. **192**, 2845–2873 (2003)
40. Sadd, M.H.: Elasticity: theory, applications, and numerics, 2nd edn. Academic Press, Burlington (2009)
41. Selvadurai, A.P.S.: Partial differential equations in mechanics 2—The Biharmonic equation, Poisson's equation. Springer, Berlin (2000)
42. Shi, M.X., Huang, Y., Hwang, K.C.: Fracture in a higher-order elastic continuum. J. Mech. Phys. Solids **48**, 2513–2538 (2000)
43. Shodja, H.M., Tehranchi, A.: A formulation for the characteristic lengths of fcc materials in first strain gradient elasticity via the Sutton–Chen potential. Phil. Mag. **90**, 1893–1913 (2010)
44. Sneddon, I.N.: The relation between load and penetration in the axisymmetric Boussinesq problem for a punch of arbitrary profile. Int. J. Eng. Sci. **3**, 47–57 (1965)
45. Sun, L., Han, R.P.S., Wang, J., Lim, C.T.: Modeling the size-dependent elastic properties of polymeric nanofibers. Nanotechnology **19**, 455706-1∼8 (2008)
46. Toupin, R.A.: Elastic materials with couple-stresses. Arch. Ration. Mech. Anal. **11**, 385–414 (1962)
47. Toupin, R.A.: Theory of elasticity with couple-stress. Arch. Rat. Mech. Anal. **17**, 85–112 (1964)
48. Vardoulakis, I., Exadaktylos, G., Aifantis, E.: Gradient elasticity with surface energy: mode-III crack problem. Int. J. Solids Struct. **33**, 4531–4559 (1996)
49. Wang, G.F., Feng, X.Q.: Effects of surface stresses on contact problems at nanoscale. J. Appl. Phys. **101**, 013510–1∼6 (2007)
50. Yang, F., Chong, A.C.M., Lam, D.C.C., Tong, P.: Couple stress based strain gradient theory for elasticity. Int. J. Solids Struct. **39**, 2731–2743 (2002)
51. Yang, F.Q.: Analysis of the axisymmetric indentation of a semi-infinite piezoelectric material: the evaluation of the contact stiffness and the effective piezoelectric constant. J. Appl. Phys. **103**, 074115–1∼8 (2008)
52. Zhou, D., Jin, B.: Boussinesq–Flamant problem in gradient elasticity with surface energy. Mech. Res. Commun. **30**, 463–468 (2003)
53. Zhou, S.-S., Gao, X.-L.: Solutions of half-space and half-plane contact problems based on surface elasticity. Z. Angew. Math. Phys. (published on-line) (2012). doi: 10.1007/s00033-012-0205-0
54. Zhou, S.-S., Gao, X.-L., He, Q.-C.: A unified treatment of axisymmetric adhesive contact problems using the harmonic potential function method. J. Mech. Phys. Solids **59**, 145–159 (2011)

Xin-Lin Gao
Department of Mechanical Engineering
University of Texas at Dallas
800 West Campbell Road
Richardson, TX 75080-3021
USA
e-mail: Xin-Lin.Gao@utdallas.edu

Song-Sheng Zhou
Department of Mechanical Engineering
Texas A&M University
College Station, TX 77843-3123
USA

Present Address:
Song-Sheng Zhou
Houston Technology Center
Baker Hughes Inc.
2001 Rankin Road
Houston, TX 77073
USA

(Received: September 27, 2012)